Source apportionment of fine organic carbon (OC) using receptor modelling at a rural site of Beijing

Wu, Xuefang; Chen, Chunrong; Vu, Tuan V.; Liu, Di; Baldo, Clarissa; Shen, Xiaobao; Zhang, Qiang; Cen, Kuang; Zheng, Mei; He, Kebin; Shi, Zongbo; Harrison, Roy M.

DOI:
10.1016/j.envpol.2020.115078

Document Version
Peer reviewed version

Citation for published version (Harvard):
Wu, X, Chen, C, Vu, TV, Liu, D, Baldo, C, Shen, X, Zhang, Q, Cen, K, Zheng, M, He, K, Shi, Z & Harrison, RM 2020, 'Source apportionment of fine organic carbon (OC) using receptor modelling at a rural site of Beijing: insight into seasonal and diurnal variation of source contributions', *Environmental Pollution*, vol. 266, no. Part 1, 115078, pp. 115078. https://doi.org/10.1016/j.envpol.2020.115078

Source Apportionment of Fine Organic Carbon (OC) Using Receptor Modelling at a Rural Site of Beijing: Insight into Seasonal and Diurnal Variation of Source Contributions

Xuefang Wu[1,2], Chunrong Chen[3], Tuan V. Vu[1], D. Liu[1] Clarissa Baldo[1], Xiaobao Shen[4], Qiang Zhang[3], Kuang Cen[2] Mei Zheng[5], Kebin He[6,7], Zongbo Shi[1], and Roy M. Harrison[1*†]

[1]Division of Environmental Health and Risk Management
School of Geography, Earth and Environmental Sciences
University of Birmingham
Edgbaston, Birmingham B15 2TT, United Kingdom

[2]School of Earth Sciences and Resources
China University of Geosciences, Xueyuan Road 29, 100083 Beijing, China

[3]Ministry of Education Key Laboratory for Earth System Modeling,
Department of Earth System Science,
Tsinghua University, Beijing 100084, China

[4] School of Light Industry, Beijing Technology and Business University
Beijing 100048, China

[5]SKL-ESPC and BIC-ESAT, College of Environmental Sciences and Engineering
Peking University, Beijing 100871, China

[6]State Environmental Protection Key Laboratory of Sources and Control of Air Pollution Complex, Beijing 100084, China

[7]State Key Joint Laboratory of Environment, Simulation and Pollution Control
School of Environment, Tsinghua University, Beijing 100084, China

[*] To whom correspondence should be addressed (Email: r.m.harrison@bham.ac.uk)

[†]Also at: Department of Environmental Sciences / Center of Excellence in Environmental Studies, King Abdulaziz University, PO Box 80203, Jeddah, 21589, Saudi Arabia

ABSTRACT

This study was designed to investigate the seasonal characteristics and apportion the sources of organic carbon during non-haze days (<75 μg m^{-3}) and haze (≥75 μg m^{-3}) events at Pinggu, a rural Beijing site. Time-resolved concentrations of carbonaceous aerosols and organic molecular tracers were measured during the winter of 2016 and summer 2017, and a Chemical Mass Balance (CMB) model was applied to estimate the average source contributions. The concentration of OC in winter is comparable with previous studies, but relatively low during the summer. The CMB model apportioned seven separate primary sources, which explained on average 73.8% on haze days and 81.2% on non-haze days of the organic carbon in winter, including vegetative detritus, biomass burning, gasoline vehicles, diesel vehicles, industrial coal combustion, residential coal combustion and cooking. A slightly lower percentage of OC was apportioned in the summer campaign with 64.5% and 78.7% accounted for. The other unapportioned OC is considered to consist of secondary organic carbon (SOC). During haze episodes in winter, coal combustion and SOC were the dominant sources of organic carbon with 23.3% and 26.2%, respectively, followed by biomass burning emissions (20%), whereas in summer, industrial coal combustion and SOC were important contributors. Diurnal contribution cycles for coal combustion and biomass burning OC showed a peak at 6-9 pm, suggesting domestic heating and cooking were the main sources of organic aerosols in this rural area. Backward trajectory analysis showed that high OC concentrations were measured when the air mass was from the south, suggesting that the organic aerosols in Pinggu were affected by both local emissions and regional transport from central Beijing and Hebei province during haze episodes. The source apportionment by CMB is compared with the results of a Positive Matrix Factorization (PMF) analysis of ACSM data for non-refractory PM_1, showing generally good agreement.

Keywords: Organic aerosols; source apportionment; CMB; ACSM-PMF; Beijing

Capsule: The organic carbon in Beijing $PM_{2.5}$ is apportioned to eight sources with a Chemical Mass Balance model and the results compared to other apportionment methods.

Highlights:

- Application of CMB model to organic carbon in Beijing $PM_{2.5}$
- Seven primary sources and secondary aerosol are quantified
- Winter and summer and high time resolution data analysed
- Comparison of results with ACSM/PMF data

1. INTRODUCTION

Organic aerosols (OA) generate major research interest as they negatively impact human health, degrade visibility, and impact the Earth's global radiation balance (Robinson et al., 2007; Jacobson et al., 2000). Primary OA represents those compounds that are directly emitted from sources and secondary organic aerosol (SOA) is formed through chemical oxidation of volatile organic compounds (Kanakidou et al., 2005). In the Northern China region, the annual mean concentration of OA during 2010-2014 was 28.9 μg m^{-3} (Wu et al., 2018), which on its own far exceeds the WHO Guideline for $PM_{2.5}$. The development of effective control strategies for abating the fine organic aerosols is a high priority and thus requires a detailed understanding of the origin and atmospheric processing of organic aerosol, including recognition of emission sources and investigation of the relationships between specific aerosol components and haze episodes.

Receptor modelling is commonly used to apportion the source contributions to fine organic carbon concentrations by determining the best-fit linear combination of chemical component profiles of source aerosols and the measured ambient samples composition (Watson, 1984). One approach is the Chemical Mass Balance (CMB) model, with primary organic tracer measurements in ambient air and known source profiles (Robinson et al., 2006). CMB is well able to determine the sources if suitable source profiles are available as inputs to the model, but does not directly identify the contribution of SOA and other unknown sources (Hopke, 2015). Positive Matrix Factorization (PMF) has also been employed extensively for the source apportionment of fine OC and submicron OA and thus offers the potential to apportion directly components to source-related factors and estimate the contribution to ambient samples based on tracer species (Shrivastava et al., 2007; Viana et al., 2008).

In the past decade, much effort has been dedicated to investigate the chemical characteristics and sources of organic aerosols in Beijing, which provides useful information for effective air quality management (Lyu et al., 2019; Cao et al., 2017; Sun et al., 2015; Liu et al., 2016; Tan et al., 2014; Tang et al., 2018). For example, based on a CMB model, Wang et al. (2009) estimated that the contribution of biomass burning to OC in urban Beijing was dominant in winter with a 26% contribution to ambient OC, and that the contributions from coal combustion (17.2%) and cooking (17.3%) were comparable. In summer, the main source for OC was Other OC (usually interpreted as SOC) with 51.4%, followed by cooking (23.8%). Guo et al. (2012) collected 12h aerosol samples and found that mobile sources were dominant in rural Beijing (Yufa), with 14.7% of OC emitted from diesel engines and 8.0% of OC from gasoline, followed by biomass burning (8.9%) and coal combustion (7.7%) via the CMB model. The OC values from biomass burning and coal combustion at a rural site were slightly higher than those in urban Beijing due to more burning activities in rural areas. A number of studies reported source apportionment of fine OC in Beijing based on a PMF model. Elser et al. (2016) conducted PMF analysis on mass spectral data measured by AMS (aerosol mass spectrometry) and concluded that coal combustion and SOA were significant sources of fine OA with 46.8% and 25% contributions, respectively, during haze episodes (OA: 103 μg m^{-3}) in urban Beijing, followed by biomass burning (13.8%). During non-haze days (OA: 42 μg m^{-3}), the contributions of coal combustion and cooking increased to 55.2% and 11.5%, respectively, consistent with previous studies (Huang et al., 2014; Zhang et al., 2014). A study conducted by Zhou et al. (2018) on submicron organic aerosol sources at high altitudes in winter in Beijing, indicated that SOA is a dominant source of OA during both the heating season (72%) and non-heating season (58-64%), which were about 15-34% higher than that at ground level. Coal combustion showed a large increase during the heating period with 13-21%. These findings illustrated that combustion activities and secondary formation have a major influence on the increase of OC.

Until now, a quantitative understanding of the diurnal and seasonal variation of fine OC in rural Beijing is still incomplete. Therefore, in this study, we analyzed $PM_{2.5}$ samples collected during the APHH-China field campaigns in the winter 2016 to summer 2017 in rural Beijing (Pinggu) (Shi et al., 2019) to determine the concentration of organic molecular marker compounds. A CMB model with organic tracers was used to apportion the primary OC (POC) based on the source profiles of POC from emission sources. The diurnal and seasonal trends of source contributions to OC were compared with those from submicron organic aerosols with PMF modelling. In addition, a back trajectory clustering analysis was used to further investigate the influence of local emissions and regional transport on ambient organic aerosols.

2. METHODOLOGY

2.1 Aerosol Sampling

The sampling site (40.17 °N, 117.05 °E) is located in Pinggu at the junction point of Beijing, Tianjin, and Hebei province, approximately 60 km away from Beijing downtown. The site is in a village with surrounds of trees and farmland, 500 m east of the provincial highway (which runs north-south). It is near the residential area and far from industrial sources. The sampling was conducted from 10th November to 21st December 2016 and 22 May to 24 June 2017 as part of the Atmospheric Pollution and Human Health in a Chinese megacity (APHH-China) field campaigns (Shi et al., 2019).

Fine aerosol samples were collected on pre-fired quartz fiber filters three-hourly during haze days ($PM_{2.5}\geq75$ μg m^{-3}) and daily during non-haze days ($PM_{2.5}<75$ μg m^{-3}) using a high volume air sampler (H1000-H, Tianhong, Wuhan) at a flow rate of 1.05 m^3 min^{-1} in winter. In summer, four-hourly samples were collected during moderately polluted days ($PM_{2.5}$=35-75 μg m^{-3}) and 24 h ambient $PM_{2.5}$ samples on "clean" days ($PM_{2.5}\leq35$ μg m^{-3}). Quartz fibre filters (Pall-flex, 2500QAT-UP) were

wrapped with aluminum foil and then baked at 450 °C for 6 h before sampling. The exposed filters were stored in a refrigerator at -80 °C before being weighed and analyzed. The quartz filters were then analyzed for organic tracers, OC/EC and ion species. An additional medium volume air sampler (Thermo Scientific Partisol 2025i) was applied to collect both fine and coarse particles on 47 mm Teflon filters for gravimetric analysis. The detailed context of these sampling campaigns is described by Shi et al. (2019).

2.2 $PM_{2.5}$ Mass and Chemical Analysis

2.2.1 $PM_{2.5}$ mass, OC and EC measurement

$PM_{2.5}$ mass was determined by subtracting the weight of the Teflon filters before and after sampling using a Sartorius model MC5 microbalance. Filters were equilibrated at a constant temperature (20±2 °C) and relative humidity (< 40%) prior to weighing.

A DRI multi-wavelength Thermal-Optical carbon (Model 2015) analyser was used for quantifying the levels of OC and EC based on the EUSAAR_2 transmittance protocol (Chen et al., 2015). Organic carbon on a segment of filter (0.5 cm^2) is volatilised initially under a non-oxidizing temperature ramp from ambient to 650°C, generating four carbon fractions: OC1, OC2, OC3, and OC4. The volatilised compounds then pass through manganese dioxide (as an oxidiser) to convert them to CO_2, which is quantified by a nondispersive infrared (NDIR) CO_2 detector. A fraction of the OC pyrolyzes to EC (OP), which is estimated by the transmittance laser. Seven modulated diode lasers measure the transmittance through filter at wavelengths of 405, 450, 532, 635, 780, 808, and 980 nm; the 635 nm laser approximates the He/Ne laser that is conventionally employed to correct for pyrolysis charring of OC into EC. The second temperature ramp is from 500 to 850 °C with He/O_2 mixture carrier gas, which oxidizes the elemental carbon and pyrolysis products. Given this, the OC was defined as

OC1+OC2+OC3+OC4+OP, EC as EC1+EC2+EC3+EC4-OP. The limits of detection of OC and EC in this study were estimated to be 0.03 μg m^{-3}.

2.2.2 Quantification of individual organic compounds

Organic tracers were analyzed based on the methods of Yin at al. (2010; 2015), including 12 n-alkanes C_{24}-C_{35}, 9 hopanes, 23 PAHs, 3 anhydrosugars, 6 fatty acids and cholesterol. In brief, a 9 cm^2 of quartz filter was cut from a whole filter and then spiked with internal standards before extraction, including octacosane-d58, hexatriacontane-d74, aaa-20R-cholestane-d4, acenaphthylene-d8, phenanthrene-d10, fluoranthrene-d10, pyrene-d10, chrysene-d12, benzo(a)pyrene-d12, dibenzo(a,b)anthracene-d14, benzo(ghi)perylene-d12, phthalic 3,4,5,6-d4 acid, heptadecanoic acid-d33, heptanedioic acid-d4, methyl-beta-D-xylopyranoside, and cholesterol-2,2,3,4,4,6-d6. Filters were extracted with two 30 ml mixture of DCM and methanol (2:1, v: v, HPLC grade) while undergoing mild shaking treatment (15 min). The combined extract solution was concentrated with a rotary evaporator to approximately 5 ml, and then filtered and further concentrated to a volume of 300 μl under a stream of nitrogen. An aliquot of 50 μl extract solution was evaporated down to near dryness. To derivatise the compounds of interests, N,O-bis(trimethylsilyl)-trifluoroacetamide plus 1% trimethylchlorosilane (BSTFA+1% TMCS) and pyridine was then added. The solution is kept at 70°C for 3 h, and cooled in a desiccator for 30 mins. Another aliquot of 100 μl solution was derivatised with 2.0 M trimethylsilyldiazomethane to convert organic acids to methyl esters. A third sub-sample was utilized to analyze non-polar compounds such as n-alkanes, hopanes and PAHs directly.

Organic compounds were analyzed with a gas chromatography mass spectrometry system (GC/MS) on an Agilent Technologies instrument (GC-6890N plus MSD-5973N) fitted with a HP-5MS column

(30 m length, 0.25 mm diameter, 0.25 μm thickness). Internal standards were used to estimate recovery rates and blank values were subtracted during the quantification. Aliquots of 1 μl were injected into the GC in splitless mode. Recoveries of the quantified organic compounds were in a range of 80-110 %. Field blank filters were used as part of the quality assurance, and showed that the contamination levels were less than 5% of real samples for the species detected.

2.2.3 Receptor modeling with Chemical Mass Balance (CMB) model

To quantify the source contributions of carbonaceous aerosols, the US EPA CMB8.2 software was applied for receptor modelling. The effective variance least squares solution was applied, which uses the uncertainties in the source profiles and the ambient samples as weighting factors in the CMB solution. The source profiles were mostly obtained from work conducted in China (Table S1), including biomass burning (Zhang et al., 2007), diesel and gasoline vehicles (Cai et al., 2017), industrial and residential coal combustion (Zhang et al., 2008), and cooking (Zhao et al., 2015), except for the profile of vegetative detritus (Rogge et al., 1993). To ensure adequate model operation, we defined certain acceptance criteria for running the CMB before a minimum number of fitting species is selected. For example, some organic tracers were used to control the quality, using acceptance criteria as 0.8-1.2 for the calculated to measured ratios (C/M) for all fitting species. Moreover, quality controls were carried out requiring high R^2 (>0.95) and low Chi^2 (<2). The detailed method for organic marker species selection has been described by Yin et al. (2010; 2015).

2.3 Aerodyne Aerosol Chemical Speciation Monitor (ACSM) Measurements

2.3.1 ACSM aerosol sampling

A Quadrupole Aerodyne Aerosol Chemical Speciation Monitor (Q-ACSM) was deployed to measure non-refractory submicron aerosol ($NR\text{-}PM_1$) species, including organics, nitrate, sulfate, ammonium,

and chloride (Ng et al., 2011). Briefly, after coarse particle filtration and moisture removal, approximately 85 cc min^{-1} flow is efficiently sampled through a 100 μm critical orifice, with submicron particles (75–650 nm) focused into the first of three vacuum chambers via an aerodynamic lens (Liu et al., 2007). When the focused particle beam is transmitted into the final chamber, NR-PM_1 is flash-vaporized at ~600 ℃, ionized by 70 eV electron impact, and subsequently detected via a commercial quadrupole mass spectrometer. The ACSM works in two modes, i.e., filter mode and sample mode, which are automatically switched by a 3-way switching valve. In our study, 14 switching cycles were switched between the two modes, and the time resolution for the ACSM data was ~15 min with a scan from m/z 10 to 150 at 200 ms amu^{-1}.

2.3.2 ACSM data analysis

Mass concentrations of NR-PM1 species and the mass spectra of organic aerosol (OA) were analyzed with the standard data analysis software (v 1.6.1.1). The detailed procedures for ACSM data analysis can be found in Ng et al. (2011). Default values of relative ionization efficiency (RIE) were used for organic (1.4), nitrate (1.1), and chloride (1.3), while that of ammonium (8.88) and sulfate (0.94) was determined through analyzing pure ammonium nitrate and ammonium sulfate, respectively. In order to compensate for the particle loss (Matthew et al., 2008), collection efficiency (CE) was introduced to the ACSM data set. The CE value is affected by particle phase water, particle acidity and aerosol composition (Matthew et al., 2008). Here, the relative humidity (RH) is considered low because aerosol particles were dried before ACSM sampling, and the mass fraction of ammonium nitrate was observed normally below 40% during the whole period. In addition, aerosol particles have been reported slightly acidic in Beijing (Sun et al., 2016; Liu et al., 2017). Therefore 0.5 was used as the default value of CE.

The source apportionment of OA was processed using the positive matrix factorization algorithm developed by Paatero and Tapper. (1994). Similar to Sun et al. (2012) and Sun et al. (2013), we only considered PMF analysis up to m/z 120 in this study due to the large interferences on m/z 127–129 from the naphthalene signal. The spectral data and error matrices were pretreated following the procedures summarized in Ulbrich et al. (2009). Our PMF analysis was performed from two to seven factors with the rotational parameter (f_{peak}) varying from -1 to 1 (step = 0.1) via an Igor-Pro-based PMF Evaluation Tool (PET, v3.05; Ulbrich et al., 2009), and the summary on how to select the optimal PMF factor is shown in Table S2. In brief, solutions with two to four factors indicate mixing of factors to some extent, while for six-factor and seven-factor solutions, the additional factors do not have a plausible physical explanation and show the characteristics of factor splitting. Hence an optimal solution involving five factors at *f*peak=0 and Q/Q_{exp}=2.04 was determined, which is consistent with the recommendations in a previous study (Zhang et al., 2011). The optimal solution includes four primary factors, i.e., hydrocarbon-like OA (HOA), cooking OA (COA), coal combustion OA (CCOA), and biomass burning OA (BBOA), as well as one secondary factor, i.e., oxygenated OA (OOA). The five factors show distinct mass spectral profiles, diurnal cycles and time variations, indicating their different sources and/or processes (Figures 4 and S5). Meanwhile, the trend of each factor also correlates well with external tracers and associated inorganics (NO_x, NO_3, SO_4, Chloride; Li et al, 2017), e.g., HOA with NO_x, OOA with NO_3 and SO_4, CCOA with chloride (Figure S6). The detailed discussion of source apportionment of OA components is given in Section 3.4.

3. RESULTS AND DISCUSSION

3.1 Characteristics of $PM_{2.5}$ and Carbonaceous Compounds

Average concentrations of the $PM_{2.5}$, OC, EC, and molecular tracers included in the model are summarized in Table 1. The mean concentration of $PM_{2.5}$ was 136.2 μg m^{-3} in Pinggu during winter

sampling, which exceed Chinese National Ambient Air Quality Standards (GB3095-2012) (35 μg m^{-3} annually) by a factor of 4. The levels of OC at Pinggu fluctuated from 2.5-49 μg m^{-3} and 6.9-152 μg m^{-3} on non-haze days and haze days respectively in winter, with average concentrations of 15 μg m^{-3} and 52 μg m^{-3}, respectively. The average EC concentration during haze days was 5.4 μg m^{-3} which was 2.8 times higher than that during non-haze days. The overall average mass concentration of OC was 40 μg m^{-3}, whereas the EC concentration was 4.3 μg m^{-3}. The OC concentrations at the urban site (IAP) were similar to reports in previous studies, ranging from 20.6 to 36.1 μg m^{-3} during 2009 to 2011 in urban Beijing (Cheng et al., 2011; Zhang et al., 2013; Du et al., 2014). The Pinggu site is often downwind of urban Beijing during haze episodes, contributing to the relatively higher OC, as pollutants are transported from the downtown area to the rural sampling site. In addition, there is a contribution from greater biomass burning emissions for domestic heating and cooking in rural areas. Although the government has implemented policies to prohibit the field burning of residual straw, this is still used as a domestic fuel in the rural areas around Beijing (Cheng et al., 2013).

The mean OC and EC in summer were 7.4 and 0.8 μg m^{-3}, respectively, which is comparable to previous studies in the rural Beijing area during summer. Tang et al. (2018) reported that OC and EC in Changping in the summer 2016 were 8.9 and 0.7 μg m^{-3}, respectively. Slightly higher values of OC and EC were measured earlier in Yufa, with 9.4 and 2.4 μg m^{-3} (Guo et al., 2012), suggesting that the air pollution prevention and control measures may have had an effect.

3.2 Diurnal Variations of Organic Tracers During Haze Days in Winter and Summer

As shown in Figure S1, the levels of OC, EC and organic tracers showed similar diurnal trends. The highest peak of concentration for OC (76.3 μg m^{-3}), EC (9.3 μg m^{-3}) and other molecular tracers (such as 1.9 μg m^{-3} for levoglucosan) typically occurred during 6:00-9:00 pm, and followed by 3:00-6:00 pm which are typical high emission periods due to the traffic rush hour, heating and dinner time. The lowest concentrations of these pollutants were observed from 3:00-6:00 am. A weak peak was

observed in the morning. The concentrations were lower in the early afternoon but increased sharply after 3:00 pm. This suggested that the average diurnal variation of organic compounds was predominantly driven by the diurnal variation of the emission strength from biomass burning and coal combustion for domestic heating and cooking, combined with the change of meteorological condition such as boundary layer mixing height and ambient stagnation. Biomass combustion activities in rural areas after 6:00 pm for heating and cooking contributed to ambient $PM_{2.5}$ and anhydrosugar values.

In summer, $PM_{2.5}$ samples every 4 hours for 8 days were collected to observe the diurnal variation of organic compounds. This dataset showed the trends in OC seen in Figure S2, which were different in comparison with the same molecular marker compounds in haze episodes in winter. The peak concentration for OC (8.5 μg m^{-3}), EC (0.7 μg m^{-3}) and organic acids (0.7 μg m^{-3}) appeared at 6-9 pm, which is similar to that in winter. Highest levels were found for n-alkanes, hopanes and PAHs in daytime, especially in the morning rush hour for hopanes. However, lower levels in daytime were observed for levoglucosan, presumably due to more burning activities at night.

3.3 CMB Model Results

3.3.1 Source contributions to fine OC in winter and summer

The results of the CMB model for haze and non-haze days in winter and summer for source contributions to OC are presented in Table 2 and Figure 1. The measured concentrations of organic tracers used in source apportionment are summarized in Table 1. Seven primary OC sources were apportioned in Pinggu, including vegetative detritus, biomass burning, gasoline vehicles, diesel engines, industrial coal combustion (Industrial CC), residential coal combustion (Residential CC) and cooking. Using the average contributions, these account for about 73.8% and 81.2% of the organic carbon on haze and non-haze days in the winter. A slightly lower proportion of OC was apportioned in the summer with 64.5% and 78.7% on moderately polluted and “clean” days respectively.

The combined coal combustion (CC) from residential and industrial emissions made the highest contribution to OC in both winter (mean: 7.73 μg m^{-3}) and summer (mean: 3.40 μg m^{-3}), although the residential CC was the main contributor in winter and industrial CC played a more significant role in summer. Industrial CC and Residential CC contributed 1.52 μg m^{-3} (3.9%) and 8.40 μg m^{-3} (19.4%) respectively during haze episodes, and contributed 0.65 μg m^{-3} (5.2%) and 3.79 μg m^{-3} (28.7%) during the non-haze days in winter. Their contributions to OC in summer were Residential CC, 0.42 μg m^{-3} (4.3%) and Industrial CC, 3.94 μg m^{-3} (36.2%) during moderately polluted days, and reduced to 0.27 μg m^{-3} (5%) and 2.18 μg m^{-3} (37.3%) on "clean" days, respectively. The high contribution of domestic coal burning to $PM_{2.5}$ organic carbon in winter is mainly due to its widespread local use, high emission factors and low altitude at emission; for example, Zhang et al. (2008) estimated that the emission factors of OC for residential anthracite and bituminite briquettes burned in a brick stove were 470 mg kg^{-1} and 2975 mg kg^{-1}, respectively. However, the emission factor for fine OC for industrial mixed coal was 1.9 mg kg^{-1}. The diurnal trend of coal combustion-derived OC in Figure 2a showed that the peak occurred during 18:00-21:00 pm (20.9 μg m^{-3}), followed by midnight with 14.2 μg m^{-3} which is a typical heating time in winter. It gradually decreased to 6.6 μg m^{-3} in early morning and remained about 10 μg m^{-3} until 3:00 pm. Similar diurnal cycles of PM_1 coal combustion organic aerosol in winter Beijing were reported with the maximum value reached at midnight at 18 μg m^{-3} due to heating activities and the partitioning of semi-volatile water-soluble organic compounds from the gas phase to aerosol by the higher humidity (Sun et al., 2013). The diurnal pattern of coal combustion OC during summer (Figure 2b) was comparable to that during winter, which peaked during 16:00-20:00 with 9.0 μg m^{-3} and decreased to 2.0-4.5 μg m^{-3} during other periods. This feature may be attributable to the small number of samples (two samples) collected on low pollution days ($PM_{2.5}$<35 μg m^{-3}), and is consistent with the industrial emissions coming from the southwest (Hebei province) by advection.

Biomass burning is an important source of $PM_{2.5}$ pollution in Beijing, especially in the rural areas where straw is burned in the field or combusted indoors for cooking and heating (Duan et al., 2004;

Chen et al., 2017). In this study, OC from biomass burning (BB) was lower than the contribution from coal combustion in both seasons. The average biomass burning contribution to fine OC in winter was 8.36 μg m^{-3} on haze days and 2.59 μg m^{-3} on non-haze days accounting for 20% of the OC concentration. In summer, the average contribution of BB decreased to 1.27 μg m^{-3} (11.6%) during moderately polluted days and 0.74 μg m^{-3} (14.8%) during "clean" days. This is comparable with the CMB results from previous studies; Wang et al. (2009) estimated that the biomass burning contributed approximately 26% and 11% to fine OC in winter and summer, respectively. Tang et al. (2018) and Guo et al. (2012) estimated that the biomass burning source accounted for 8.9% at Changping and 5.0% at Yufa in summer. The higher BB contribution to OC in winter shows the influence of the burning activities in the rural area during the haze episodes. Stricter control of biomass burning in June 2017 did see a reduced impact of biomass burning on air quality (Vu et al., 2019).

There is a clear trend for higher values on average during early evening and lower values during daytime in winter from biomass burning contributions (Figure 2a). The highest average value of 21.4 μg m^{-3} (30%) occurred during 3:00-9:00 pm, whereas the lowest contribution (2.8 μg m^{-3} (17.3%)) was during the early morning. This diurnal variation was similar to that of EC and the biomass-burning tracer levoglucosan (Figure S1), which was slightly different from results observed in northwestern China, for example in Lanzhou. Xu et al. (2016) estimated that biomass burning contributed to up to approximately 20% to organic aerosol during the night but went down to 5% in the afternoon. Our result suggested that the diurnal profile of OC was predominantly driven by the variation of the emission strength from biomass burning and coal combustion for domestic heating and cooking, combined with the change of meteorological conditions such as boundary layer mixing height and ambient stagnation.

Traffic emissions including gasoline and diesel vehicle engines accounted for a lower proportion of the fine OC concentration with 18.9% (7.98 μg m^{-3}) on haze days and 15.9% (2.02 μg m^{-3}) on non-

haze days during the winter campaign. The contributions were 5.3% on moderately polluted days and 8.9% on "clean" days during summer, respectively, indicating that traffic is a minor but significant contributor to organic aerosol in Pinggu. This result differs from the finding by Tang et al. (2018) where the vehicular exhaust was a dominant primary OC source with a contribution of 37.6% at a rural site (Changping) in the summer of 2016 and thus might highlight the importance of strict control measures. The diurnal variation of vehicle emissions shows that the highest traffic contribution occurred during 3:00-9:00 pm and lowest during 3:00-6:00 am, while the concentration increased from 6:00 am, consistent with a typical rush hour-related pattern. A subordinate peak during 12:00-3:00 am might have resulted from the Beijing traffic regulations (i.e., allowing heavy-duty vehicles only to enter the 6^{th} Ring Road from midnight to 6:00 am). Traffic-derived OC exhibited slightly different diurnal trends in summer when it maintained high levels at night due to higher emissions and a lower planetary boundary layer height, and shows a peak at noon likely due to the regional transport of rush-hour vehicle emissions from the urban area.

Chinese cooking is a non-negligible contributor to organic aerosols, especially in urban Beijing with a population of approximately 23 million and nearly 30,000 restaurants. A number of previous studies on the source contribution of cooking to submicron organic aerosol indicated a weak seasonal variation, with contributions of 16-30% in summer and 13-20% in winter (Wang et al., 2009; Xu et al., 2016; Sun et al., 2013; Zhang et al., 2014). In our study, cooking emissions contributed 3.0% of OC in winter and 5.9% in summer, which are comparable with that (5.8%) estimated by Elser et al. (2016) for the extreme haze periods in winter Beijing. The reason for the lower proportion in this study may be that their sampling site was far away from the residential areas. In both seasons, the cooking source showed a similar trend with peaks at lunchtime (between noon and 2:00 pm) and dinner times (from 6:00 to midnight). A small increase in cooking OA was also observed in the morning, consistent with breakfast time, suggesting an important role of the cooking source for organic aerosols. By

applying the PMF-AMS technique, Hu et al. (2016) estimated that the cooking organic aerosol contributed 45% and 35% of total OA in PM_1 in Beijing during noon and late evening, respectively.

Vegetative detritus made a similar contribution to OC during the winter and summer campaigns with their average contribution of 8.3% (2.87 μg m^{-3}) and 7.6%, respectively, which are much higher than those in winter (0.5%) and summer (0.3%) from urban Beijing reported by Wang et al. (2009), probably because the sampling site in Pinggu is located in the village surrounded by numerous trees and plants. The source apportionment of vegetative detritus depends on the distribution of n-alkane isomers, which was derived from the anthropogenic emissions (mainly C_{16-25}) and biogenic sources (mainly C_{26-32}). Therefore, the carbon preference index (CPI) was utilized to infer the sources of n-alkanes, where a CPI larger than 3 indicates the dominance of biogenic sources (Alves et al., 2001). In this study, the average CPI for n-alkanes was 1.6 in winter and 3.5 in summer with insignificant variation between haze episodes and non-haze days. Based on the diurnal pattern in Figure 3, vegetative detritus contributes more organic carbon in the nighttime than during daytime.

"Other OC" represents OC unexplained by the CMB model. It was calculated as the difference between the measured OC and the sum of OC from all known sources calculated from CMB. This is considered as the secondary organic aerosol (SOA) and other organic species that are not accounted for in the modelling. The mean Source Contribution Estimate (SCE) of other OC was observed to be lower in mass and percentage during non-haze days (18.8% and 2.4 μg m^{-3}) and higher during haze days (26.2% and 10.7 μg m^{-3}) in winter. Other OC concentration in summer are lower, but represent a higher percentage of OC mass with 21.3% (1.14 μg m^{-3}) during "clean" days and 35.5% (4.1 μg m^{-3}) during moderately polluted days, which agreed well with the previous results from rural Beijing with 20.2-38.4% in summer (Guo et al., 2012; Tang et al., 2018). Wang et al. (2009) also estimated that the SOC could contribute about 22% in winter and 44% in summer in urban Beijing. Secondary OC is

affected by the high temperature that enhances biogenic VOC emissions and by more rapid SOA formation via active photochemical processes in summer.

3.3.2 Comparison of SOC concentration calculated by EC-tracer method with Other OC

Based on the assumption that EC comes from primary aerosol and that the POC/EC ratio is relatively constant (Turpin and Huntzicker, 1995; Castro et al., 1999), the EC-tracer method provides an independent estimate of SOC, that is as follows:

$$SOC_{EC} = OC-(POC/EC)*EC$$

where SOC_{EC} is secondary organic carbon in the ambient air, whereas POC/EC is the ratio in primary aerosol used as tracer for the evaluation of the origin of ambient organic aerosol. In this study, the POC/EC ratio was determined based on the lowest 5% sub-set of measured OC/EC ratios for the winter and summer campaigns according to the approach reported by Pio et al. (2011).

In order to verify the relationship among other OC components, secondary organic compounds, and secondary inorganic compounds in winter, the SOC_{EC}, total NO_3^-, and SO_4^{2-} are plotted along with Other OC calculated by CMB in Figure 3a. Similar trends are shared by both Other OC and NO_3^-, likely suggesting that these components were formed under similar conditions in winter (Yin et al., 2010). The Other OC is well correlated with SOC_{EC} (R^2 = 0.71 and 0.89 for winter and summer) (Figure 3b and c), confirming that "other OC" is associated with secondary organic aerosols. The substantial intercept in Figures 3b and c suggest that the EC tracer method has probably not identified the true OC/EC ratio for primary emissions due to an absence of periods without a secondary contribution.

3.4 Comparison of the CMB Results with the Source Contribution of Submicron OA Estimated by ACSM-PMF

Five organic components in NR-PM_1 were identified based on the mass spectra (as shown in Figure 4) measured in winter at Pinggu, including HOA, CCOA, BBOA, COA, and OOA. The ideal factor numbers and the diagnostics of the PMF model error estimates is elaborated in Supplementary Information (SI) (Figure S3, S4 and Table S2). Source apportionment of OA was obtained based on the OC contribution and the various OA/OC ratios of different sources. In order to compare with the source apportionment results from the CMB model for fine OC, the OA concentrations from the ACSM-PMF were converted to a concentration of organic carbon. The OA/OC ratios used for this comparison were taken from values measured in Beijing, i.e. 1.38 for COA/COC (cooking organic carbon), 1.58 for BBOA/BBOC (biomass burning organic carbon) (Xu et al., 2019), 1.35 for CCOA/CCOC (coal combustion organic carbon), 1.31 for HOA/HOC (hydrocarbon-like organic carbon) (Sun et al., 2016), and 1.78 for OOA (Huang et al., 2010).

The HOA factor shows a similar spectrum to that of traffic or other fossil fuel combustion, which has a profile dominated by alkyl fragment signatures, the $C_nH_{2n+1}^+$ (m/z 29, 43, 57) and $C_nH_{2n-1}^+$ (m/z 27, 41, 55) ion series (Figure 4). There is a strong correlation (R^2=0.82) between the time series of HOA and that of NO_x, a tracer of vehicle emissions. The average HOC concentrations are 7.46 μg m^{-3} during haze days and 2.42 μg m^{-3} on non-haze days, respectively, which was close to the CMB estimates for both diesel and gasoline vehicles (Figure 5). The diurnal pattern of HOC shows peaks during morning and evening rush hours (Figure 6), further supporting the association of HOC with traffic activities. This is also consistent with the result of CMB.

The mass spectrum of CCOA presented high signals at m/z 41, 43, 55, 57, 69, 91, and an especially significant peak at m/z 115 (Figure 4). Moreover, a strong relationship (R^2=0.81) between CCOA and chloride is observed. The contribution of CCOC shows a similar percentage to coal combustion estimated by CMB, contributing 24.7% (8.9 μg m^{-3}) on haze days and 28.4% (3.3 μg m^{-3}) on non-haze days (Figure 5). The diurnal variation in CCOC is characterized by low mass levels at daytime and high levels related to the heating (17-21:00 local time) at night. This is consistent with the results estimated by CMB (Figure 6). The contributions of both coal combustion and vehicle emissions to OA based on AMS observations (Xu et al., 2019) are lower than those in Pinggu.

The profile of the BBOA factor was characterized by prominent peaks at m/z 60 and 73 as tracers of biomass burning aerosol. The time series of BBOA correlates well with the peak of m/z 60 (R^2=0.99). The contribution of BBOC to OC indicated a smaller fraction than the sum of biomass burning and vegetation detritus contributions estimated by CMB, with an average of 16.1% (5.8 μg m^{-3}) of OC on haze days and 11.9% (1.4 μg m^{-3}) on non-haze days. The apparent underestimation of BBOC contributions to submicron OC in the PMF model may result from an over-estimation of COC, because the cooking emissions contributes more to fine particles (Du et al., 2017). Moreover, the size distribution of OA emitted from biomass burning can grow rapidly during regional transport. Both the CCOC concentrations and the variation in the CMB biomass burning estimate show lower concentrations during daytime and higher levels during nighttime.

The COA factor profile is generally identified by significant peaks at m/z 55 (i.e. $C_3H_3O^+$, $C_4H_7^+$) and 57 (i.e. $C_3H_5O^+$, $C_4H_9^+$), typically seen in the spectral pattern of OA from fresh cooking emissions (Mohr et al., 2012). Moreover, the diurnal variation of the COC factor presents distinctive peaks at lunch and dinner times, resembling that of the CMB result. The contribution of COC (19.3%) reported by PMF is higher than that in fine OC of the CMB model and the COA contribution in urban Beijing

(15%) (Xu et al., 2019). Dall'Osto et al. (2015) have highlighted the uncertainties inherent in COA estimates determined at rural sites.

The OOA profile is identified from the prominent peak at m/z 44. Moreover, there are relatively strong correlations between the OOA factor and those of secondary inorganic species, such as sulfate and nitrate (R^2=0.86 and 0.93, respectively). The OOC accounted for a higher fraction with 20% (7.0 μg m^{-3}) during haze days than the 14.8% contribution (1.7 μg m^{-3}) attributed to submicron OA during non-haze days, consistent with the result of CMB with 25% on haze days and 18% on non-haze days, respectively. However, the contribution of SOA in urban Beijing can be considerably higher, for example, approximately 52% (Xu et al., 2019), which was attributed to photochemical reactions and aqueous-phase processing (Wang et al., 2019). Like the diurnal pattern of Other OC in the CMB model, the OOC concentration increases gradually from the morning to late afternoon, indicating their formation from photo-chemical processing (Figure 6).

The full results of the ACSM-PMF analysis appear alongside the CMB results in Table 2. To assist a direct comparison, Table 3 shows the same set of data in generic categories which should be comparable between the methods. In most cases the comparison, expressed as percentages as the samples are of different size ranges ($PM_{2.5}$ for CMB and PM_1 for ACSM-PMF), is rather close. One major divergence is that the CMB method attributes a significant amount of mass to the vegetative detritus category which is not reported by the ACSM. It is unclear to what factor this will be attributed by the ACSM-PMF. It is rich in hydrocarbons which would match aspects of the HOA mass spectrum, but would be expected to show a different temporal pattern to vehicle emitted HOA. The other divergence is in the estimates of cooking emissions. This is one of the more difficult source categories to estimate by receptor modelling (Reyes-Villegas et al., 2018). There is evidence that typical ACSM-PMF data analyses may over-estimate COA by a factor of around two (Yin et al., 2015; Reyes-Villegas et al., 2018), but this would not be sufficient to explain the discrepancy.

Dall'Osto et al. (2015) suggest that the PMF may fail to make a good separation of COA from HOA, leading to errors, but this would not be likely to account for the large differences seen in Table 2. Abdullahi et al. (2018) have shown that in a UK urban context, estimates of cooking aerosol by CMB are not strongly sensitive to the source profiles used, so use of an unrepresentative source profile may not be the explanation.

3.5 Back Trajectory Analysis

In order to identify the influence of local emissions or regional transport on the organic aerosols, the 3-day air mass back trajectories (HYSPLIT) were calculated as shown in Figure 7 terminating at 100, 500 and 1000 metres. Figure 7a shows that the clean air masses mainly come from the northwest sector or pass over the sea. On the contrary, during haze days, the main air mass passed through the area south of Pinggu (including Hebei, Shandong and Anhui) and urban Beijing with dense industry and population (Figure 7b). Combined with the lower wind speed (0.8 m s^{-1}), the particulate matter was less diluted and more SOA could be produced. Consequently, the organic aerosols in Pinggu were affected not only by local emissions during haze episodes, but also received a major contribution from regional transport.

4. CONCLUSIONS

Seven primary OC sources were apportioned in Pinggu by CMB, including vegetative detritus, biomass burning, gasoline vehicle emissions, diesel vehicles, industrial coal combustion, residential coal combustion and cooking, contributing on average about 73.8% on haze days and 81.2% on non-haze days of OC in winter. A slightly lower percentage of OC was apportioned in the summer with 64.5% and 78.7% on moderately polluted and "clean" days. Combustion activities and secondary formation are dominant sources of OC at Pinggu in both cold and hot seasons. In wintertime, coal combustion emissions contributed 24-34% of OC, followed by SOC (18-25%), biomass burning

(20%), motor vehicles (16-19%), vegetative detritus (8.3%) and cooking (3%). In summer, these sources accounted for 36-37%, 21-35%, 11.6-14.8%, 5.3-8.9%, and 7.6% of OC respectively.

The source apportionment of submicron organic aerosol by a PMF model of ACSM data at Pinggu in winter gave estimates of OOC (20.1%), CCOC (27.5%), COC (16.6%), HOC (19.9%), and BBOC (15.9%). There is reasonable agreement between the CMB results and those of PMF analysis. Both methods illustrated that coal combustion and SOC are the dominant sources of OA and indicated an important biomass burning contribution. However, the cooking contribution estimated by CMB is lower than the PMF likely due to different particle size for analysis, or difficulties with the ACSM-PMF technique (Dall'Osto et al., 2015). The diurnal variations of the CMB source estimates agree well with those from the ACSM-PMF data and fit logically with the expected variations in source activity and meteorology. These results for a rural site outside of the main Beijing urban area complement the many published receptor modelling studies for sites within urban Beijing, although due to recent implementation of pollution control measures in the city, the pattern of source contributions is rapidly changing (Vu et al., 2019).

DATA AVAILABILITY

Data supporting this publication are openly available from the UBIRA eData repository at https://doi.org/10.25500/edata.bham.00000389

ACKNOWLEDGEMENT

This research was funded by the UK Natural Environment Research Council (NERC) and the Chinese Natural Science Funding Council (NSFC) as part of the APHH-Beijing study (NE/N007190/1). XW acknowledges additional support from the China Scholarship Council (CSC).

REFERENCES

Abdullahi, K.L., Delgado-Saborit, J.M., Harrison, R.M., 2018. Sensitivity of a chemical mass balance model for $PM_{2.5}$ to source profiles for differing styles of cooking. Atmos. Environ., 178, 282-285.

Alves, C., Pio, C., Duarte, A., 2001. Composition of extractable organic matter of air particles from rural and urban portuguese areas. Atmos. Environ., 35, 5485-5496.

Cai, T., Zhang, Y., Fang, D., Shang, J., Zhang, Y., Zhang, Y., 2017. Chinese vehicle emissions characteristic testing with small sample size: Results and comparison. Atmos. Pollut. Res., 8, 154-163.

Cao, F., Zhang, Y., Ren, L., Liu, J., Li, J., Zhang, G., Liu, D., Sun, Y., Wang, Z., Shi, Z., 2017. New insights into the sources and formation of carbonaceous aerosols in China: Potential applications of dual carbon isotopes. Nat. Sci. Rev., 4, No. 6, https://doi.org/10.1093/nsr/nwx097.

Castro, L., Pio, C., Harrison, R.M., Smith, D., 1999. Carbonaceous aerosol in urban and rural european atmospheres: Estimation of secondary organic carbon concentrations. Atmos. Environ., 33, 2771-2781.

Chen, J., Li, C., Ristovski, Z., Milic, A., Gu, Y., Islam, M. S., Wang, S., Hao, J., Zhang, H., He, C., 2017. A review of biomass burning: emissions and impacts on air quality, health and climate in China. Sci. Tot. Environ., 579, 1000-1034.

Chen, L. W. A., Chow, J. C., Wang, X. L., Robles, J. A., Sumlin, B., Lowenthal, D. H., Zimmermann, R., Watson, J. G. 2015. Multi-wavelength optical measurement to enhance thermal/optical analysis for carbonaceous aerosol. Atmos. Meas. Tech., 8, 451–461.

Cheng, Y., Engling, G., He, K.-B., Duan, F.-K., Ma, Y.-L., Du, Z.-Y., Liu, J.-M., Zheng, M., Weber, R. J., 2013. Biomass burning contribution to Beijing aerosol. Atmos. Chem. Phys., 13, 7765-7781.

Cheng, Y., He, K.B., Duan, F.K., Zheng, M., Du, Z.Y., Ma, Y.L., Tan, J.H., 2011. Ambient organic carbon to elemental carbon ratios: Influences of the measurement methods and implications. Atmos. Environ., 45, 2060-2066.

Dall'Osto, M., Paglione, M., Decesari, S., Facchini, M.C., O'Dowd, C., Plass-Duellmer, C., Harrison, R.M., 2015. On the origin of AMS "Cooking Organic Aerosol" at a rural site. Environ. Sci. Technol., 49, 13964-13972.

Du, Z., He, K., Cheng, Y., Duan, F., Ma, Y., Liu, J., Zhang, X., Zheng, M., Weber, R., 2014. A yearlong study of water-soluble organic carbon in Beijing I: Sources and its primary vs. secondary nature. Atmos. Environ., 92, 514-521.

Du, W., Zhao, J., Wang, Y., Zhang, Y., Wang, Q., Xu, W., Chen, C., Han, T., Zhang, F., Li, Z., Fu, P., Li, J., Wang, Z., Sun, Y., 2017. Simultaneous measurements of particle number size distributions at ground level and 260 m on a meteorological tower in urban Beijing, China. Atmos. Chem. Phys., 17, 6797-6811.

Duan, F., Liu, X., Yu, T., Cachier, H., 2004. Identification and estimate of biomass burning contribution to the urban aerosol organic carbon concentrations in Beijing. Atmos. Environ., 38, 1275-1282.

Elser, M., Huang, R.-J., Wolf, R., Slowik, J. G., Wang, Q., Canonaco, F., Li, G., Bozzetti, C., Daellenbach, K.R., Huang, Y., Zhang, R., Li, Z., Cao, J., Baltensperger, U., El-Haddad, I., Prévôt, A.S.H., 2016. New insights into $PM_{2.5}$ chemical composition and sources in two major cities in China during extreme haze events using aerosol mass spectrometry. Atmos. Chem. Phys., 16, 3207-3225.

Guo, S., Hu, M., Guo, Q., Zhang, X., Zheng, M., Zheng, J., Chang, C. C., Schauer, J.J., Zhang, R., 2012. Primary sources and secondary formation of organic aerosols in Beijing, China. Environ. Sci. Technol., 46, 9846-53.

Hopke, P.K., 2015. It is time to drop principal components analysis as a "receptor model". J. Atmos. Chem., 72, 127-128.

Hu, W., Hu, M., Hu, W., Jimenez, J.L., Yuan, B., Chen, W., Wang, M., Wu, Y., Chen, C., Wang, Z., 2016. Chemical composition, sources, and aging process of submicron aerosols in Beijing: Contrast between summer and winter. J. Geophys. Res. Atmospheres, 121, 1955-1977.

Huang, R.J., Zhang, Y., Bozzetti, C., Ho, K. F., Cao, J.J., Han, Y., Daellenbach, K.R., Slowik, J.G., Platt, S.M., Canonaco, F., Zotter, P., Wolf, R., Pieber, S. M., Bruns, E.A., Crippa, M., Ciarelli, G., Piazzalunga, A., Schwikowski, M., Abbaszade, G., Schnelle-Kreis, J., Zimmermann, R., An, Z., Szidat, S., Baltensperger, U., El Haddad, I., Prevot, A.S., 2014. High secondary aerosol contribution to particulate pollution during haze events in China. Nature, 514, 218-22.

Huang, X.F., He, L.Y., Hu, M., Canagaratna, M.R., Sun, Y., Zhang, Q., Zhu, T., Xue, L., Zeng, L. W., Liu, X.G., Zhang, Y.H., 2010. Highly time-resolved chemical characterization of atmospheric submicron particles during 2008 Beijing Olympic Games using an Aerodyne High-Resolution Aerosol Mass Spectrometer. Atmos. Chem. Phys., 10, 8933-8945.

Jacobson, M.C., Hansson, H.C., Noone, K.J., Charlson, R.J., 2000. Organic atmospheric aerosols: Review and state of the science. Rev. Geophys., 38, 267-294.

Kanakidou, M., Seinfeld, J., Pandis, S., Barnes, I., Dentener, F., Facchini, M., Dingenen, R.V., Ervens, B., Nenes, A., Nielsen, C., 2005. Organic aerosol and global climate modelling: A review, Atmos. Chemi.Phys., 5, 1053-1123.

Li, H.Y., Zhang, Q., Chen, C. R., Wang, L.T., Wei, Z., Zhou, S., Parworth, C., Zheng, B., Canonaco, F., Prévôt, A. H., Chen, P., Zhang, H.L., He, K.B., 2017. Wintertime aerosol chemistry and haze evolution in an extremely polluted city of North China Plain: Significant contribution from coal and biomass combustions. Atmos. Chem. Phys., 17, 4751-4768.

Liu, M.X., Song, Y., Zhou, T., Xu, Z.Y., Yan, C.Q., Zheng, M., Wu, Z.J., Hu, M., Wu, Y.S., Zhu, T., 2017. Fine particle pH during severe haze episodes in northern China, J. Geophys. Res. Lett., 44, 5213-5221.

Liu, J., Li, J., Liu, D., Ding, P., Shen, C., Mo, Y., Wang, X., Luo, C., Cheng, Z., Szidat, S., 2016. Source apportionment and dynamic changes of carbonaceous aerosols during the haze bloom-decay process in China based on radiocarbon and organic molecular tracers. Atmos. Chem. Phys., 16, 2985-2996.

Liu, P.S.K., Deng, R., Smith, K. A., Williams, L.R., Jayne, J.T., Canagaratna, M.R., Moore, K., Onasch, T.B., Worsnop, D.R., and Deshler, T., 2007. Transmission efficiency of an aerodynamic

focusing lens system: Comparison of model calculations and laboratory measurements for the aerodyne aerosol mass spectrometer. Aerosol Sci. Technol., 41, 721-733.

Lyu, R., Shi, Z., Alam, M. S., Wu, X., Liu, D., Vu, T. V., Stark, C., Xu, R., Fu, P., Feng, Y., 2019. Alkanes and aliphatic carbonyl compounds in wintertime $PM_{2.5}$ in Beijing, China. Atmos. Environ., 202, 244-255.

Matthew, B.M., Middlebrook, A.M., Onasch, T.B., 2008. Collection efficiencies in an aerodyne aerosol mass spectrometer as a function of particle phase for laboratory generated aerosols. Aerosol Sci.Technol., 42, 884-898.

Mohr, C., DeCarlo, P.F., Heringa, M.F., Chirico, R., Slowik, J. G., Richter, R., Reche, C., Alastuey, A., Querol, X., Seco, R., Peñuelas, J., Jiménez, J.L., Crippa, M., Zimmermann, R., Baltensperger, U., Prévôt, A.S.H., 2012. Identification and quantification of organic aerosol from cooking and other sources in Barcelona using aerosol mass spectrometer data, Atmos. Chem. Phys., 12, 1649-1665.

Ng, N.L., Herndon, S.C., Trimborn, A., Canagaratna, M.R., Croteau, P., Onasch, T.M., Sueper, D., Worsnop, D.R., Zhang, Q., Sun, Y.L., Jayne, J. T., 2011An aerosol chemical speciation monitor (ACSM) for routine monitoring of the composition and mass concentrations of ambient aerosol. Aerosol Sci.Technol., 45, 780-794.

Paatero, P., Tapper, U., 1994. Positive matrix factorization: A nonnegative factor model with optimal utilization of error estimates of data values. Environmetrics, 5, 111-126.

Pio, C., Cerqueira, M., Harrison, R.M., Nunes, T., Mirante, F., Alves, C., Oliveira, C., De La Campa, A.S., Artíñano, B., Matos, M., 2011. OC/EC ratio observations in europe: re-thinking the approach for apportionment between primary and secondary organic carbon. Atmos. Environ., 45, 6121-6132.

Reyes-Villegas, E., Bannan, T., Le Breton, M., Mehra, A., Priestly, M., Percival, C., Coe, H., Allan, J.D., 2018. Online chemical characterization of food-cooking organic aerosols: Implications for source apportionment. Environ. Sci. Technol., 52, 5308-5318.

Robinson, A.L., Donahue, N.M., Shrivastava, M.K., Weitkamp, E.A., Sage, A.M., Grieshop, A.P., Lane, T.E., Pierce, J.R., Pandis, S.N., 2007. Rethinking organic aerosols: semivolatile emissions and photochemical aging. Science, 315, 1259-1262.

Robinson, A.L., Subramanian, R., Donahue, N.M., Bernardo-Bricke, A., Rogge, W.F., 2006. Source apportionment of molecular markers and organic aerosol 1. Polycyclic aromatic hydrocarbons and methodology for data visualization. Environ. Sci.Technol., 40, 7803-7810.

Rogge, W.F., Hildemann, L.M., Mazurek, M.A., Cass, G.R., Simoneit, B.R., 1993. Sources of fine organic aerosol. 4. Particulate abrasion products from leaf surfaces of urban plants. Environ. Sci. Technol., 27, 2700-2711.

Shi, Z., Vu, T., Kotthaus, S., Harrison, R.M., Grimmond, S., Yue, S., Zhu, T., Lee, J., Han, Y., Demuzere, M., Dunmore, R.E., Ren, L., Liu, D., Wang, Y., Wild, O., Allan, J., Acton, W.J., Barlow, J., Barratt, B., Beddows, D., Bloss, W.J., Calzolai, G., Carruthers, D., Carslaw, D.C., Chan, Q., Chatzidiakou, L., Chen, Y., Crilley, L., Coe, H., Dai, T., Doherty, R., Duan, F., Fu, P., Ge, B., Ge, M., Guan, D., Hamilton, J.F., He, K., Heal, M., Heard, D., Hewitt, C.N., Hollaway, M., Hu, M., Ji, D., Jiang, X., Jones, R., Kalberer, M., Kelly, F.J., Kramer, L., Langford, B., Lin, C., Lewis, A.C., Li, J., Li, W., D., Liu, H., Liu, H., Liu, J., Loh, M., Lu, K., Lucarelli, F., Mann, G., McFiggans, G., Miller, M.R., Mills, G., Monk, P., Nemitz, E., O'Connor, F., Ouyang, B., Palmer, P.I., Percival, C.,

Popoola, O., Reeves, C., Rickard, A.R., Shao, L., Shi, G., Spracklen, D., Stevenson, D., Sun, Y., Sun, Z., Tao, S., Tong, S., Wang, Q., Wang, W., Wang, X., Wang, X., Wang, Z., Wei, L., Whalley, L., Wu, X., Wu, Z., Xie, P., Yang, F., Zhang, Q., Zhang, Y., Zhang, Y., Zheng, M., 2019. In-depth study of air pollution sources and processes within beijing and its surrounding region (APHH-Beijing). Atmos. Chem.Phys., 19, 7519-7546.

Shrivastava, M.K., Subramanian, R., Rogge, W.F., Robinson, A. L., 2007. Sources of organic aerosol: positive matrix factorization of molecular marker data and comparison of results from different source apportionment models. Atmos. Environ., 41, 9353-9369.

Sun, Y., Du, W., Fu, P., Wang, Q., Li, J., Ge, X., Zhang, Q., Zhu, C., Ren, L., Xu, W., Zhao, J., 2016. Primary and secondary aerosols in Beijing in winter: sources, variations and processes. Atmos. Chem. Physics, 16, 8309-8329.

Sun, Y., Wang, Z., Du, W., Zhang, Q., Wang, Q., Fu, P., Pan, X., Li, J., Jayne, J., Worsnop, D., 2015. Long-term real-time measurements of aerosol particle composition in Beijing, China: Seasonal variations, meteorological effects, and source analysis. Atmos. Chemi.Phys., 15, 10149-10165.

Sun, Y.L., Wang, Z.F., Fu, P.Q., Yang, T., Jiang, Q., Dong, H.B., Li, J., Jia, J.J., 2013. Aerosol composition, sources and processes during wintertime in Beijing, China. Atmos. Chem. Phys., 13, 4577-4592.

Sun, Y., Wang, Z., Dong, H., Yang, T., Li, J., Pan, X., Chen, P., Jayne, J.T., 2012. Characterization of summer organic and inorganic aerosols in Beijing, China with an Aerosol Chemical Speciation Monitor. Atmos. Environ., 51, 250-259.

Tan, J.-H., Duan, J.-C., Chai, F.-H., He, K.-B., Hao, J.-M., 2014. Source apportionment of size segregated fine/ultrafine particle by PMF in Beijing. Atmos. Res., 139, 90-100.

Tang, R., Wu, Z., Li, X., Wang, Y., Shang, D., Xiao, Y., Li, M., Zeng, L., Wu, Z., Hallquist, M., 2018. Primary and secondary organic aerosols in summer 2016 in Beijing. Atmos. Chem.Phys., 18, 4055-4068.

Turpin, B. J., Huntzicker, J. J., 1995. Identification of secondary organic aerosol episodes and quantitation of primary and secondary organic aerosol concentrations during SCAQS. Atmos. Environ., 29, 3527-3544.

Ulbrich, I.M., Canagaratna, M.R., Zhang, Q., Worsnop, D.R., Jimenez, J.L., 2009. Interpretation of organic components from Positive Matrix Factorization of aerosol mass spectrometric data. Atmos. Chem. Phys., 9, 2891-2918.

Viana, M., Pandolfi, M., Minguillón, M., Querol, X., Alastuey, A., Monfort, E., Celades, I., 2008. Inter-comparison of receptor models for PM source apportionment: Case study in an industrial area. Atmos. Environ., 42, 3820-3832.

Vu, T.V., Shi, Z., Cheng, J., Zhang, Q., He, K., Wang, S., Harrison, R.M., 2019. Assessing the impact of clean air action on air quality trends in Beijing using a machine learning technique. Atmos. Chem. Phys., 19, 11303-11314.

Wang, Q., Shao, M., Zhang, Y., Wei, Y., Hu, M., Guo, S., 2009Source apportionment of fine organic aerosols in Beijing. Atmos. Chem.Phys., 9, 8573-8585.

Wang, Y., Chen, J., Wang, Q., Qin, Q., Ye, J., Han, Y., Li, L., Zhen, W., Zhi, Q., Zhang, Y., Cao, J., 2019. Increased secondary aerosol contribution and possible processing on polluted winter days in China. Environ. Intl., 127, 78-84.

Watson, J.G., 1984. Overview of receptor model principles. J. Air Pollut. Control Assoc., 34, 619-623 .

Wu, X., Vu, T.V., Shi, Z., Harrison, R.M., Liu, D., Cen, K., 2018. Characterization and source apportionment of carbonaceous $PM_{2.5}$ particles in China - A review. Atmos. Environ., 189, 187-212.

Xu, W., Sun, Y., Wang, Q., Zhao, J., Wang, J., Ge, X., Xie, C., Zhou, W., Du, W., Li, , Fu, P., Wang, Z., Worsnop, D. R., , H., 2019. Changes in aerosol chemistry from 2014 to 2016 in winter in Beijing: Insights from high resolution aerosol mass spectrometry. J. Geophys. Res.: Atmospheres, 124, 1132-1147.

Xu, J., Shi, J., Zhang, Q., Ge, X., Canonaco, F., Prévôt, A.S.H., Vonwiller, M., Szidat, S., Ge, J., Ma, J., An, Y., Kang, S., Qin, D., 2016. Wintertime organic and inorganic aerosols in Lanzhou, China: Sources, processes and comparison with the results during summer. Atmos. Chem. Phys., 16, 14937-14957.

Yin, J., Cumberland, S.A., Harrison, R.M., Allan, J., Young, D.E., Williams, P.I., Coe, H., 2015. Receptor modelling of fine particles in southern england using cmb including comparison with AMS-PMF factors. Atmos. Chem. Phys., 15, 2139-2158.

Yin, J., Harrison, R.M., Chen, Q., Rutter, A., Schauer, J.J., 2010. Source apportionment of fine particles at urban background and rural sites in the UK atmosphere. Atmos. Environ., 44, 841-851.

Zhang, J., Sun, Y., Liu, Z., Ji, D., Hu, B., Liu, Q., Wang, Y., 2014. Characterization of submicron aerosols during a month of serious pollution in Beijing, 2013. Atmos. Chem. Phys., 14, 2887-2903.

Zhang, R., Jing, J., Tao, J., Hsu, S.C., 2013. Chemical characterization and source apportionment of $PM_{2.5}$ in Beijing: Seasonal perspective. Atmos. Chem.Phys., 13, 7053-7074.

Zhang, Q., Jimenez, J., Canagaratna, M., Ulbrich, I., Ng, N., Worsnop, D., and Sun, Y., 2011. Understanding atmospheric organic aerosols via factor analysis of aerosol mass spectrometry: a review. Anal. Bioanalyt. Chem., 401, 3045-3067.

Zhang, Y., Schauer, J.J., Zhang, Y., Zeng, L., Wei, Y., Liu, Y., Shao, M., 2008. Characteristics of particulate carbon emissions from real-world Chinese coal combustion. Environ. Sci. Technol., 42, 5068-5073.

Zhang, Y.-X., Shao, M., Zhang, Y.-H., Zeng, L.-M., He, L.-Y., Zhu, B., Wei, Y.-J., Zhu, X.-L., 2007. Source profiles of particulate organic matters emitted from cereal straw burnings, J. Environ. Sci., 19, 167-175.

Zhao, X., Hu, Q., Wang, X., Ding, X., He, Q., Zhang, Z., Shen, R., Lü, S., Liu, T., and Fu, X., 2015. Composition profiles of organic aerosols from chinese residential cooking: Case study in urban Guangzhou, South China. J. Atmos. Chem., 72, 1-18.

Zhou, W., Wang, Q., Zhao, X., Xu, W., Chen, C., Du, W., Zhao, J., Canonaco, F., Prévôt, A.S.H., Fu, P., Wang, Z., Worsnop, D. R., Sun, Y., 2018. Characterization and source apportionment of

811 organic aerosol at 260 m on a meteorological tower in Beijing. China, Atmos. Chem.Phys., 18,
812 3951-3968.
813

TABLE LEGENDS

Table 1. Summary of measured concentrations at Pinggu in winter and summer.

Table 2. Source contribution estimates (μg m^{-3}) for fine particulate OC in winter and summer at Pinggu.

Table 3. Comparison of CMB and ACSM-PMF results for haze days and clear days expressed in generic categories.

FIGURE LEGENDS

Figure 1. Source contributions to fine OC in winter and summer Pinggu. (a) haze days and non-haze days in winter; (b) diurnal variation of source contribution to OC during haze days in winter; (c) moderately polluted and "clean" days in summer; (d) diurnal variation of source contribution of OC during moderately polluted days in summer.

Figure 2. Diurnal variation of OC from different sources estimated by the CMB model.

Figure 3. Time series of mean values for Other OC, SOC-EC, NO_3^- and SO_4^{2-} (a); Secondary component comparison at Pinggu showing relationship between estimated secondary OC from tracer EC method (SOC-EC) and the CMB model in winter (b) and summer (c).

Figure 4. Mass spectra of five organic aerosol factors including HOA, CCOA, BBOA, COA, OOA.

Figure 5. Comparison of the average source contribution of submicron organic aerosol by PMF model and the sources of fine OA estimated by CMB model in winter Pinggu. OA refers to the organic aerosol in PM_1 and OC means organic carbon in $PM_{2.5}$.

Figure 6. Diurnal patterns of PM_1 organic compound factors (unit: μg m^{-3}) (The plots show the mean values and 95% confidence interval in the mean).

Figure 7. (a) Backward trajectory ending at 00:00 UTC 21 November 2016, winter non-haze day. (b) Backward trajectory ending at 08:00 UTC December 2016, winter haze day. (c) Backward trajectory ending at 00:00 UTC 11 June 2017, summer good day. (d) Backward trajectory ending at 00:00 UTC 17 June 2017, summer moderately polluted day. The authors gratefully acknowledge the NOAA Air Resources Laboratory (ARL) for the provision of the HYSPLIT transport and dispersion model (http://www.ready.noaa.gov).

852 **Table 1**. Summary of measured concentrations at Pinggu in winter and summer.

853

Compounds	Non-haze days (N=38)[a]			Haze days (N=89)[a]			Summer (N=81)		
	Range	Mean	STD	Range	Mean	STD	Range	Mean	STD
$PM_{2.5}$[b]	9.1-72.7	42.8	20.1	77.2-587.3	206.8	104.9	9.5-79.7	28.7	15.4
OC[b]	2.5-49.0	15.3	10.6	6.9-152.0	52.3	29.3	1.2-20.4	7.4	4.4
EC[b]	0.2-7.2	1.9	1.6	0.6-20.7	5.4	3.6	0.1-3.2	0.8	0.8
OC/EC	1.6-25.2	9.8	3.9	5.5-20.6	10.7	3.4	1.7-19.6	8.2	4.2
$OC/PM_{2.5}$	5.9-68.1%	36.4%	16.9%	4.6-65.4%	26.3%	11.0%	4.2-64%	26.7%	12.0%
SOC[b,c]	1.2-15.7	7.1	3.7	3.8-96.4	25.5	17	1.0-18.1	5.2	3.5
C24	2.4-40.9	15.1	11.0	5.8-128	51.3	32.1	0.5-6.7	1.4	1.0
C25	3.2-47.4	17.1	11.8	8.2-143.9	54.8	33.7	0.1-18.1	4.1	3.0
C26	1.9-31.8	11.3	7.8	5.9-95.7	36.6	20.9	0.2-9	1.4	1.2
C29	4.1-110.5	20.4	21.9	9.3-195.3	64.8	47.7	0.1-164.5	22.7	27.7
C31	2.5-36.6	9.3	6.8	2.6-74.1	23.9	16.9	0.1-47.7	6.1	8.2
C33	2.7-65.8	14.5	12.5	3.4-103.2	29.3	20.7	1.4-54.9	5.4	6.1
C35	1.8-21.5	8.1	5.3	3.3-33.8	15.2	7.3	0.2-3.2	1.1	0.7
CPI	1.0-3.3	1.6	0.5	0.8-3.3	1.5	0.4	0.6-12	3.9	2.8
17α-22,29,30-Trisnorhopane	0.8-5.8	3.1	1.9	0.8-9.1	3.6	2.0	0.2-1	0.5	0.2
17β,21α-30-norhopane	0.8-8	3.9	2.3	1.0-11.2	4.7	2.4	0.3-5	1.9	1.2
17α(H),21β(H)-hopane	0.8-6.8	3.7	2.3	0.9-10.8	4.3	2.4	0.2-3.2	1.3	0.9
Fluorene	0.9-36.3	8.0	6.0	1.8-230.7	24.6	43.3	0.1-29.8	2.3	3.7
Phenanthene	0.2-114	18.8	19.2	5.3-204.3	40.6	39.3	0.1-1.6	0.6	0.3
Anthracene	0.1-61	9.9	9.6	2.0-84.5	17.7	15.8	0.01-1.4	0.2	0.2
Fluorathene	4.8-170.9	25.1	27.5	7.9-243.1	56.7	48.9	0.1-1.7	0.6	0.4
Pyrene	2.2-177	24.4	29.1	6.1-244.8	54.0	47.6	0.1-2.1	0.7	0.4
Benzo[a]anthrane	1.0-158.4	19.3	25.8	2.8-175.4	42.5	31.2	0.5-2.7	1.3	0.4
Chrysene	1.5-126.3	17.6	20.3	5.4-143.1	42.3	28.2	0.1-1.8	0.6	0.4
Benzo[b]fluorathene	0.8-62.8	12.0	11.2	4.7-104.1	28.3	19.5	0.1-4.6	1.2	0.9
Benzo[k]fluorathene	0.1-90.5	13.0	14.8	4.0-103.0	30.8	19.4	0.2-5.6	1.4	0.9
Benzo[e]pyrene	0.3-32.1	5.7	5.5	2.1-46.4	14.0	8.4	0.001-1.1	0.3	0.3
Benzo[a]pyrene	0.3-32.2	5.8	5.8	1.5-55.0	14.5	10.2	0.003-1.1	0.3	0.2
Indeno[1,2,3-cd]pyrene	0.1-23.4	5.0	4.3	1.0-43.4	11.6	8.2	0.002-1.9	0.6	0.4
Dibenzo[a,b]anthracene	0.2-4.4	1.2	0.9	0.1-18.5	2.8	2.5	0.1-0.4	0.2	0.1
Picene	0.1-2.4	0.8	0.7	0.1-7.1	2.1	1.6	0.002-0.5	0.2	0.1
Benzo[ghi]perylene	0.4-36.9	6.6	6.3	2.7-55.3	15.7	10.2	0.002-2	0.5	0.4
Coronene	0.2-4.5	1.7	1.2	0.3-11.7	3.9	2.9	0.003-0.7	0.2	0.2
Levoglucosan	28.9-1396	348.9	320.5	108.1-4418	1082.9	838.1	16.9-327.1	74.5	56.9
Cholesterol	0.2-6.5	1.3	1.4	0.1-10.8	2.0	2.0	0.01-2.1	0.4	0.4
Palmitic acid	1.5-607.9	128.7	134.2	8.0-1283.6	314.7	280.9	33-582	189.3	123.7
Oleic acid	0.4-346.1	80.9	84.9	1.6-1433.2	172.4	263.1	4.6-63.1	18.4	10.4
Linoleic acid	1.9-277.6	92.7	82.1	0.1-1075.1	161.6	205.1	0.9-76.7	25.4	14.8
Stearic acid	3.9-396.3	124.0	109.0	5.0-1614.5	263.4	273.3	7.4-592.7	80.2	94.2

854 (a) The non-haze days and haze days in winter; (b) The unit is μg m^{-3}; (c) SOC concentration is calculated by EC-
855 tracer method. The unit of molecular organic markers is ng m^{-3}.

856 The table includes data with different sampling intervals (see Methods). The mean values, ranges and standard
857 deviations derive mainly from the shorter sampling intervals.

858
859

Table 2. Source contribution estimates (μg m^{-3}) for fine particulate OC and submicron OC in winter and summer at Pinggu.

Sources	Winter-daily		Winter-3 hours	Summer-daily		Summer-4 hours
CMB results	Haze days	Clear days		Moderately polluted days	"clean" days	
Vegetative Detritus	4.13	0.98	2.07	0.36	0.19	0.82
Biomass Burning	8.36	2.59	10.7	1.27	0.74	2.21
Gasoline vehicle	1.19	0.52	1.87	0.11	0.07	0.07
Diesel vehicle	6.79	1.5	4.59	0.43	0.41	0.52
Industrial CC	1.52	0.65	3.53	3.94	2.18	3.4
Residential CC	8.4	3.79	7.34	0.42	0.27	0.58
Cooking	0.9	0.45	1.28	0.51	0.35	1.17
Other OC	10.7	2.36	11	4.06	1.14	8.47
Fine OC	42.0	12.8	42.4	11.1	5.35	17.2
AMS-PMF (winter)	Haze days	Clear days				
BBOC	5.82	1.38				
COC	6.95	2.78				
HOC	7.46	2.42				
CCOC	8.90	3.29				
OOC	6.96	1.71				
Submicron OC	36.1	11.6				

Haze days in winter: $PM_{2.5}$≥75 μg m^{-3}; Non-haze days in winter: $PM_{2.5}$≤75 μg m^{-3};
Moderately polluted days in summer: $PM_{2.5}$≥35 μg m^{-3}; "clean" days in summer: $PM_{2.5}$≤35 μg m^{-3}.

867 **Table 3**. Comparison of CMB and ACSM-PMF results for haze days and clear days expressed in
868 generic categories.
869

Source Category	Haze days (%)		Clear days (%)	
	CMB	**ACSM-PMF**	**CMB**	**ACSM-PMF**
Biomass burning/BBOC	19.9	16.1	20.2	11.9
Gasoline & diesel vehicle/HOC	19.0	20.7	15.8	20.9
Industrial & residential/CC/CCOC	23.6	24.7	34.7	28.4
Cooking/COC	2.1	19.3	3.5	24.0
Other/OOC	25.5	19.3	18.4	14.7
Vegetative detritus/-	9.8	-	7.7	-

870
871

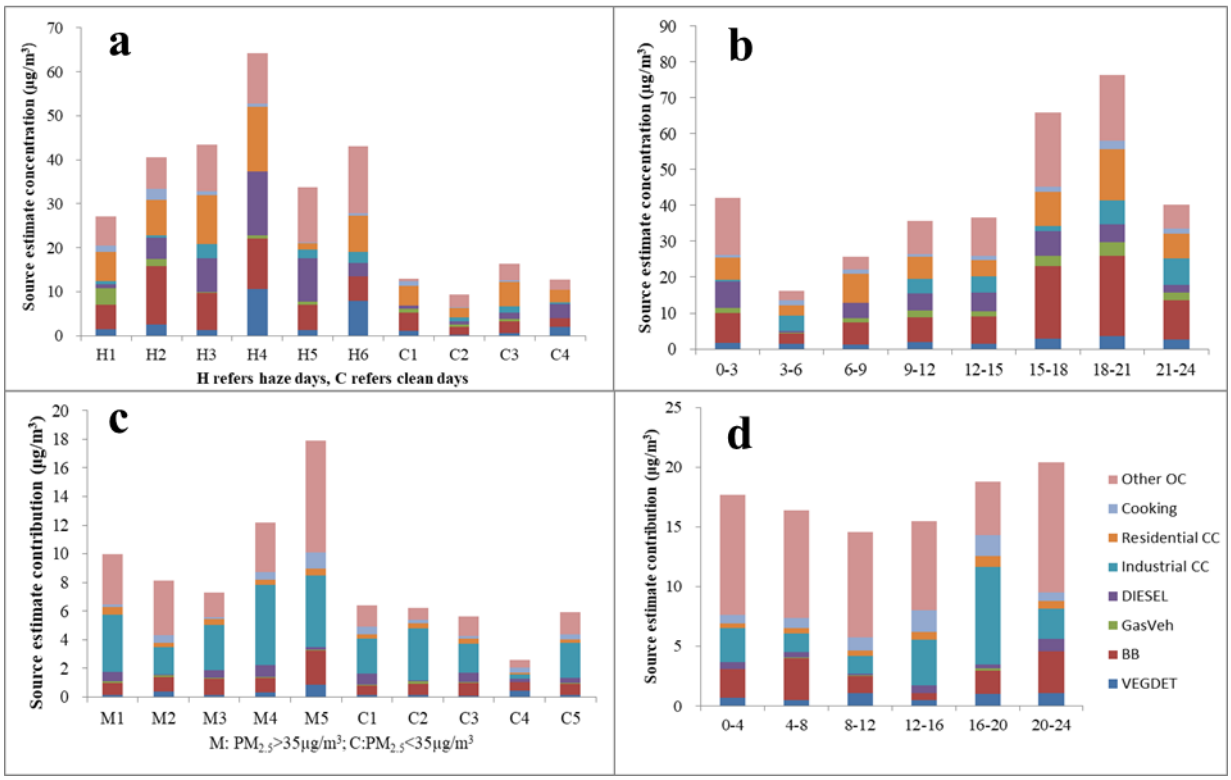

VegDet: Vegetative Detritus, BB: Biomass Burning, GasVeh: Gasoline vehicle.

Figure 1. Source contributions to fine OC in winter and summer Pinggu. (a) haze days and non-haze days in winter; (b) diurnal variation of source contribution to OC during haze days in winter; (c) moderately polluted and "clean" days in summer; (d) diurnal variation of source contribution of OC during moderately polluted days in summer.

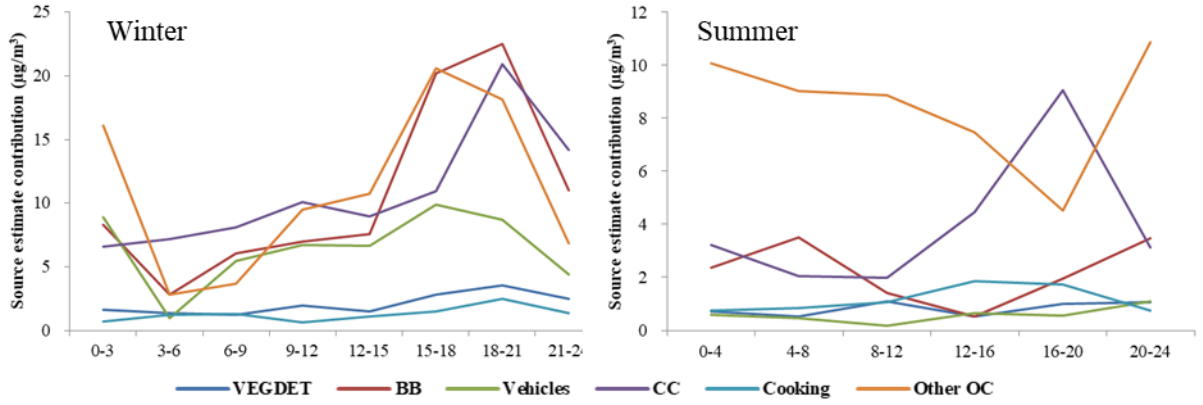

Figure 2. Diurnal variation of OC from different sources estimated by the CMB model.

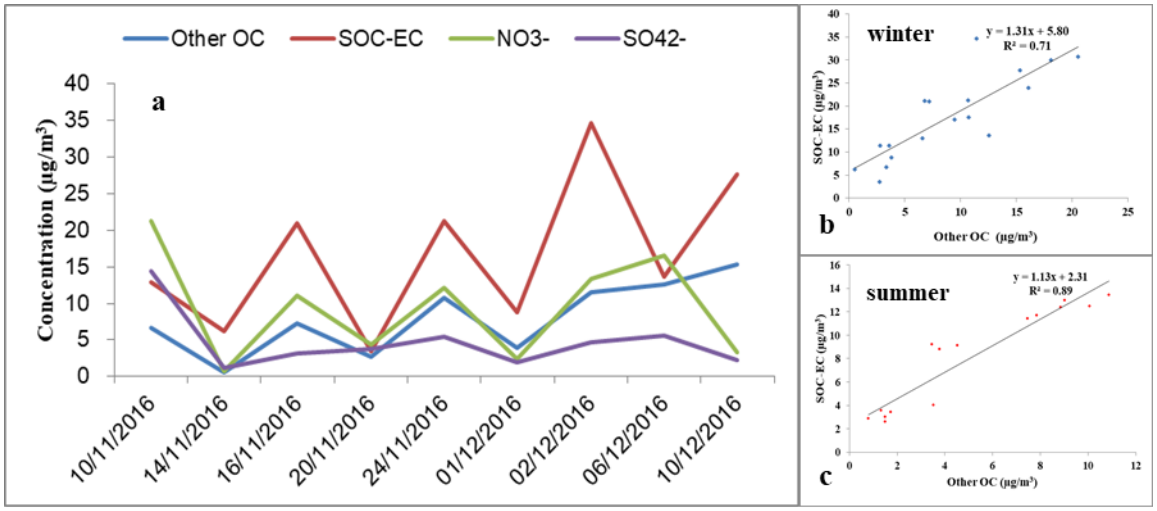

Figure 3. Time series of mean values for Other OC, SOC-EC, NO_3^- and SO_4^{2-} (a); Secondary component comparison at Pinggu showing relationship between estimated secondary OC from tracer EC method (SOC-EC) and the CMB model in winter (b) and summer (c).

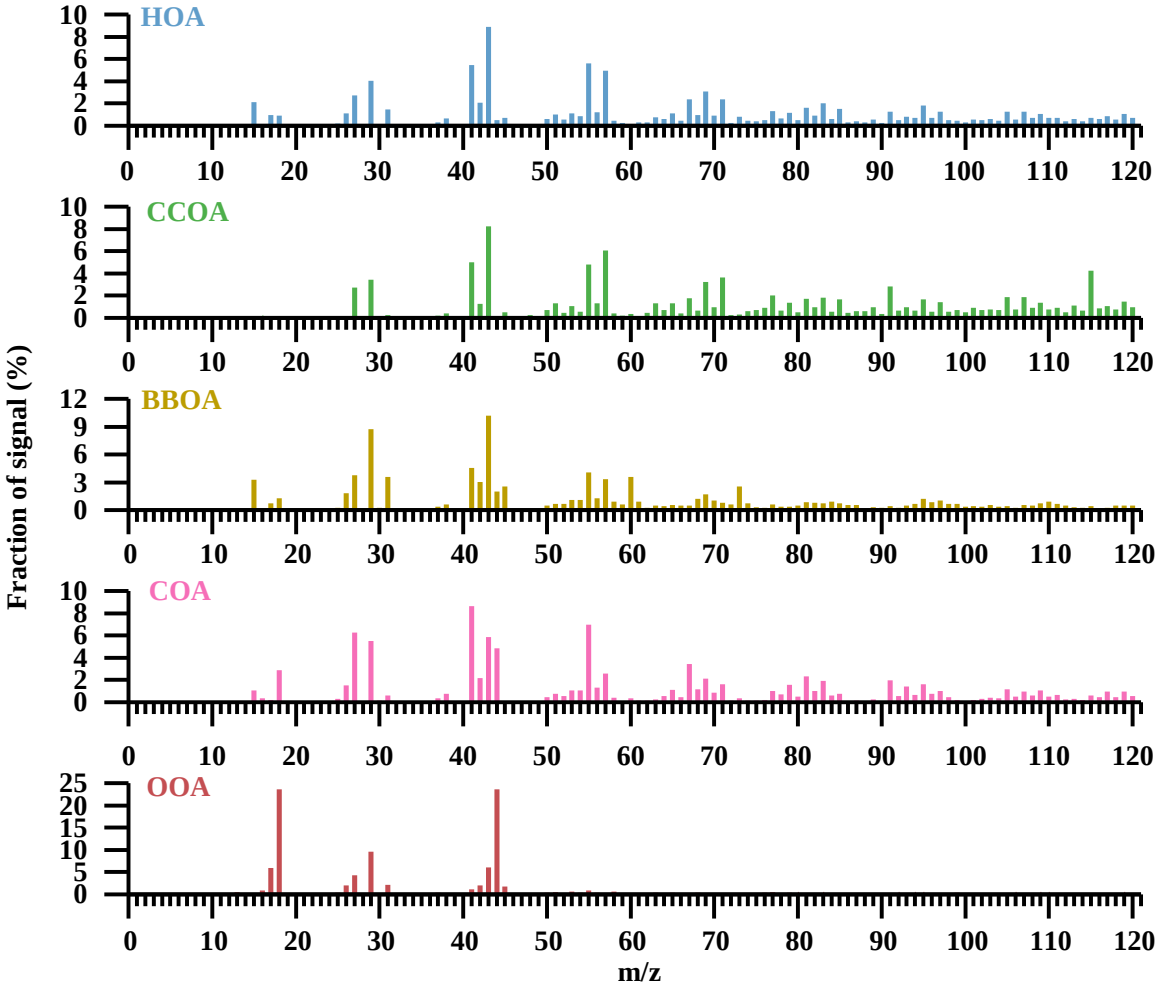

Figure 4. Mass spectra of five organic aerosol factors including HOA, CCOA, BBOA, COA, OOA.

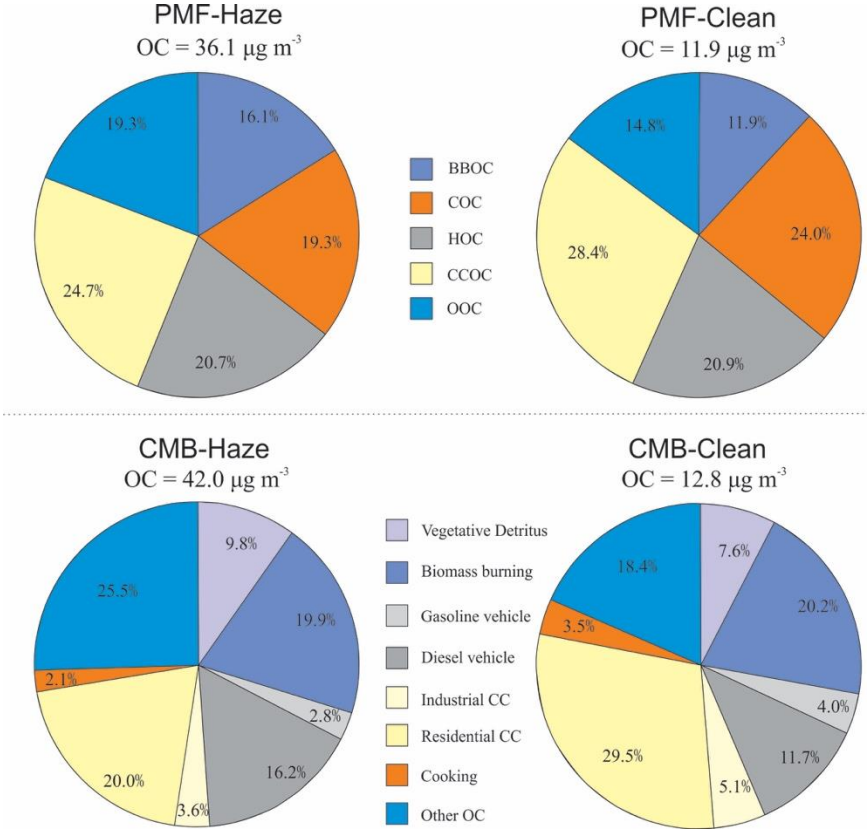

910

911 **Figure 5.** Comparison of the average source contribution of submicron organic aerosol by PMF
912 model and the sources of fine OA estimated by CMB model in winter Pinggu. Both datasets
913 expressed as OC.
914

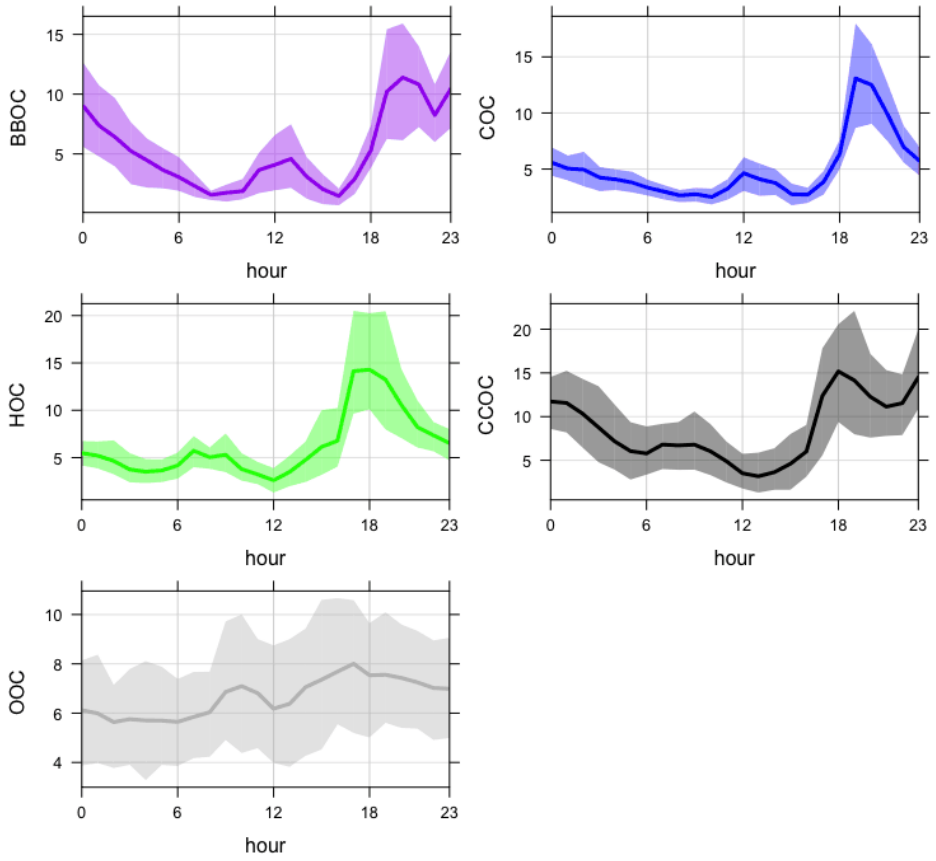

Figure 6. Diurnal patterns of PM_1 organic compound factors (unit: µg m^{-3}) (The plots show the mean values and 95% confidence interval in the mean).

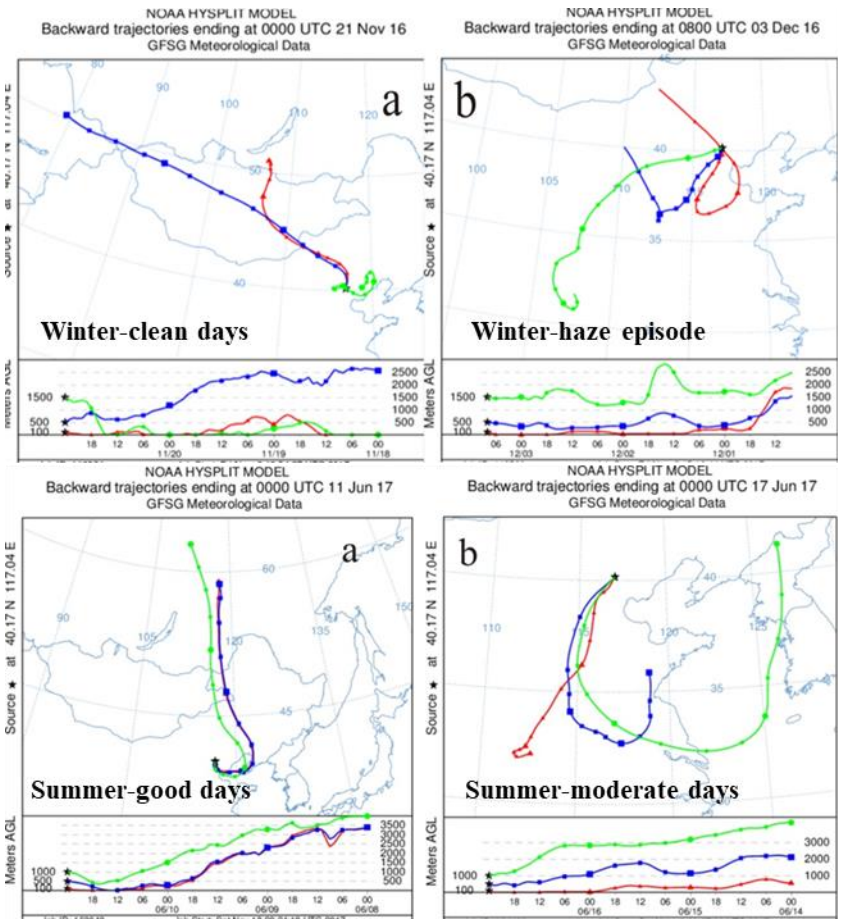

Figure 7. (a) Backward trajectory ending at 00:00 UTC 21 November 2016, winter non-haze day. (b) Backward trajectory ending at 08:00 UTC December 2016, winter haze day. (c) Backward trajectory ending at 00:00 UTC 11 June 2017, summer good day. (d) Backward trajectory ending at 00:00 UTC 17 June 2017, summer moderately polluted day. The authors gratefully acknowledge the NOAA Air Resources Laboratory (ARL) for the provision of the HYSPLIT transport and dispersion model (http://www.ready.noaa.gov).